



## Displacement field and slip distribution of the 2005 Kashmir earthquake from SAR imagery

E. Pathier,<sup>1</sup> E. J. Fielding,<sup>2</sup> T. J. Wright,<sup>1</sup> R. Walker,<sup>1</sup> B. E. Parsons,<sup>1</sup> and S. Hensley<sup>2</sup>

Received 10 June 2006; revised 9 August 2006; accepted 14 September 2006; published 24 October 2006.

[1] The 8th October 2005 Kashmir Earthquake  $M_w$  7.6 involved primarily thrust motion on a NE-dipping fault. Sub-pixel correlation of ENVISAT SAR images gives the location of the 80 km-long fault trace (within 300–800 m) and a 3D surface displacement field with a sub-metric accuracy covering the whole epicentral area. The slip distribution inverted using elastic dislocation models indicates that slip occurs mainly in the upper 10 km, between the cities of Muzaffarabad and Balakot. The rupture reached the surface in several places. In the hanging wall, horizontal motions show rotation from pure thrust to oblique right-lateral motion that are not observed in the footwall. A segmentation of the fault near Muzaffarabad is also suggested. North of the city of Balakot, slip decreases dramatically, but a diffuse zone of mainly vertical surface displacements, which could be post-seismic, exists further north, where most of the aftershocks occur, aligned along the NW-SE Indus-Kohistan Seismic Zone. **Citation:** Pathier, E., E. J. Fielding, T. J. Wright, R. Walker, B. E. Parsons, and S. Hensley (2006), Displacement field and slip distribution of the 2005 Kashmir earthquake from SAR imagery, *Geophys. Res. Lett.*, 33, L20310, doi:10.1029/2006GL027193.

### 1. Introduction

[2] On 8th October 2005, a  $M_w$  7.6 earthquake occurred in northern Pakistan in the mountainous Kashmir region (Figure 1) causing more than 80,000 deaths. The Kashmir earthquake (also called the Pakistan Earthquake) is the latest in a series of large historical earthquakes located along the southern front of the Himalaya [Bilham, 2004]. The moment tensor solutions from Harvard and the USGS National Earthquake Information Center (NEIC) were available on the web a few hours after the earthquake, rapidly followed by the first slip models from seismological data (e.g., Martin Vallée, <http://www-geoazur.unice.fr/SEISME/PAKISTAN081005/note1.html>; Yuji Yagi, [http://www.geo.tsukuba.ac.jp/press\\_HP/yagi/EQ/2005Pakistan](http://www.geo.tsukuba.ac.jp/press_HP/yagi/EQ/2005Pakistan)), indicating a NE-dipping fault with primarily thrust motion. On 2 November, we made available a more precise fault location established from sub-pixel correlation of Synthetic Aperture Radar (SAR) images ([http://comet.nerc.ac.uk/news\\_kashmir.html](http://comet.nerc.ac.uk/news_kashmir.html)). This preliminary analysis was done within a few days after the first suitable post-event

ENVISAT SAR acquisition, thanks to efforts of the European Space Agency (ESA) who made these data available as soon as possible. Using a similar approach, *Fujiwara et al.* [2006] showed that location of the highest displacement gradient match pre-existing fault traces previously mapped by *Nakata et al.* [1991].

[3] First analyses from seismology and remote-sensing suggested a large amount of shallow slip, locally in excess of 6 m, explaining the intensity of damage and number of casualties, and revealed heterogeneity in the slip distribution and possibly segmentation of the fault. The fault is located at the western end of the Himalaya, at the Hazara Syntaxis, where an old major geologic boundary of the range, the Main Boundary Thrust (MBT), bends around by 180°. The fault trace runs from Bagh to Balakot via the Jhelum river valley and the city of Muzaffarabad (Figure 1). In its northern part, it follows the MBT trace along the southwestern boundary of the Hazara syntaxis. The fault is also aligned with a zone of seismicity recorded by the Tarbela Seismic Network in 1973–1976, called the Indus-Kohistan Seismic Zone (IKSZ) that extends some 100 km to the NW of Balakot and has been proposed to be a NE-dipping ramp [Armbruster et al., 1978]. *Parsons et al.* [2006] point out that, due to static stress changes, there is an increased stress on the IKSZ portion close to the fault, where most of the aftershocks occur. Possible structural controls over the slip distribution remain to be investigated. In this paper, we present a more extensive analysis of the surface deformation including new SAR data acquired with different geometries. These data allow us to construct a three-dimensional surface displacement field caused by the earthquake and to invert for the slip distribution on the fault plane using a homogeneous linear elastic model.

### 2. SAR Offset Data

[4] Near global coverage and all-weather, day-night capability make SAR data suitable for remote-sensing analysis of natural hazards. In this study, we used ENVISAT ASAR data (Table 1) because they have extensive coverage, high spatial resolution and the existing archive of previous acquisitions allows selection of pairs of pre- and post-event images with suitable baselines (distance separating the two orbits of a pair of images) and time interval. These last two parameters should be as small as possible when measuring coseismic displacements caused by earthquakes with SAR imagery. As shown in Figure 2, the epicentral area is well covered by three selected tracks in ascending and descending modes (i.e., satellite flying from south to north or from north to south, respectively).

[5] To measure surface deformation using SAR imagery, two main techniques are available: interferometric SAR

<sup>1</sup>Centre for the Observation and Modelling of Earthquakes and Tectonics, Department of Earth Sciences, University of Oxford, Oxford, UK.

<sup>2</sup>Jet Propulsion Laboratory, California Institute of Technology, Pasadena, California, USA.

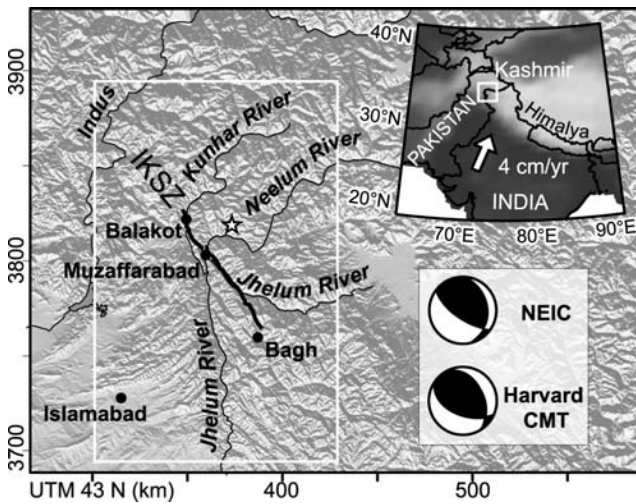


**Figure 1.** Inset: DEM showing the study area located in Kashmir at the Western Syntaxis of the Himalayan range. Main figure: shaded DEM of the Kashmir region. The star is the epicenter of the 8 October 2005 earthquake from NEIC. At about 100 km from Islamabad, the fault rupture (thick black line) runs from Balakot to Bagh via Muzaffarabad, and is aligned with the Indus-Kohistan Seismic Zone (IKSZ). Thin black lines are rivers and the white frame shows the extent of Figure 2.

(InSAR) [e.g., *Rosen et al.*, 2000] and sub-pixel image correlation [e.g., *Michel et al.*, 1999]. For the Kashmir earthquake, conventional InSAR, the most accurate technique (centimetric), can only give reliable measurement on a narrow band of the footwall in the Jhelum valley and in some far field areas where temporal and geometrical signal decorrelation (due to high topography and steep slopes) and decorrelation due to the large earthquake deformation itself are less severe. Although less accurate ( $\sim 0.2\text{--}1.0$  m), sub-pixel SAR image correlation is more robust for mountainous environments such as in Kashmir. This technique is based on measurement of line and column offset between two amplitude images. At the end of the process, two maps can be constructed for each track (Figure 2), giving two components of the displacements that occurs between the two acquisitions: one parallel to the satellite track (azimuth offset) and the other along its line of sight (range offset). Offsets have been computed using the Jet Propulsion Laboratory/California Institute of Technology ROI\_pac software [*Rosen et al.*, 2004], using overlapping matching windows of 64 by 64 pixels (i.e.,  $\sim 300$  m by  $\sim 500$  m in azimuth and range direction respectively) applied to full resolution images (4 m in azimuth, 8 m in slant range) with steps of 8 pixels in range and 16 in azimuth. Formal errors of the offset measurements are estimated from the width of the peak in the cross-correlation surface for each match. It is only a lower bound on the total error, but provides a criterion for discarding poor matches. Offsets with a formal error ( $1\sigma$ ) larger than 0.7 m and with a magnitude larger than 8 m are removed. These thresholds are based on a qualitative analysis, trying to reduce noise in the data while keeping a good data coverage. A weighted averaging procedure that uses the inverse of the variance of each

match as a weighting is applied with a window of 5 samples in range by 11 samples in azimuth. We correct estimated offsets for image distortions due to the fact that images are not acquired exactly from the same point of view. For range offsets, distortions have been modeled using a DEM and precise orbital data, and we correct for a constant shift using far field data where we assumed no coseismic displacement. For azimuth offsets, we only apply long-wavelength flattening using a quadratic surface fit. Results are geocoded at 120 m resolution in UTM zone 43 using ROI\_pac and a SRTM DEM.

[6] A clear deformation signal appears in the epicentral area (see Figure 2). The fault line oriented NW-SE is very straight in its southern portion. The largest displacements occur to the east of the fault on the hanging wall around the slightly curved north portion where the azimuth displacement shows a larger lobe than the range one. In the range offset data of ascending track 270 (data set with highest SNR), north of UTM northing 3830 km, a more diffuse zone of deformation is visible. Associated formal errors are about 0.35 m in average but vary with the geometry of acquisition, and with the topography and slopes (see auxiliary material Figure S1<sup>1</sup>). On average, due to its lower and smoother topography, footwall measurement are more accurate ( $\sim 0.30$  m) than the hanging wall ones ( $\sim 0.39$  m).

### 3. 3D Surface Displacements Map

[7] Each offset map is the projection of the full 3D displacement field in the range or azimuth direction. Where three or more such scalar components are available, it is possible to solve for the full 3D displacements field (i.e., the East, North and Up components). The resulting map (see Figure 3a) is easier to interpret than the offset maps. To construct the 3D displacement and associated formal error maps, we followed the method described by *Wright et al.* [2004]. We computed displacements only for points where azimuth and range offset data for both ascending and descending tracks are available (i.e., four to six scalar components of displacement are used for each point). Errors are propagated from formal errors in the measured offsets. The north-south component is the best constrained ( $\sigma = 0.07$  m on average in the footwall and  $\sigma = 0.13$  m in the hanging wall), while the east-west component is the least well constrained ( $\sigma = 0.19$  m on average in the footwall and  $\sigma = 0.46$  m in the hanging wall). For the vertical component,  $\sigma$  is about 0.09 m on average in the footwall and 0.20 m in the hanging wall; see auxiliary material Figure S2 for more details.

[8] Results show high gradient or discontinuity of displacement across an almost continuous 80 km-long NE-SW line that we interpret as the fault trace, the location of which can be mapped with an accuracy of  $\sim 600$  m. There is a left-step of about 1.5 km in the fault trace located just west of the area in Figure 3b, suggesting fault segmentation. This left step is located at the transition zone between the Muzaffarabad-Bagh 55 km-long straight southern portion of the fault, where the displacement across the fault is lower (with a maximum in the middle), and the curved

<sup>1</sup>Auxiliary materials are available in the HTML. doi:10.1029/2006GL027193.

**Table 1.** Details of the Six Offset Data Sets Used in This Study<sup>a</sup>

Direction	Track	Beam	Pre-Event	Start Date	End Date	⊥ Baseline, m	Azimuth (East North)	Range (East North Up)
Ascending	270	I6	5	25-06-2005	12-11-2005	60	[-0.18 -0.98]	[-0.67 -0.12 0.73]
Ascending	499	I6	4	19-09-2005	24-10-2005	270	[-0.18 -0.98]	[-0.63 -0.11 0.77]
Descending	463	I2	20	17-09-2005	26-11-2005	90	[0.21 -0.98]	[0.38 -0.08 0.92]

<sup>a</sup>Offsets are measured on pairs of ENVISAT ASAR images (in image mode) acquired before and after 8 October 2005. Each line corresponds to a pair. The number of images acquired during the two years preceding the event is given in column 4. For each pair, azimuth (component along track) and range (component along line of sight) offsets are measured. Exact orientation of these components depends on the geometry of acquisition and on the position of the measured point within the images. The last two columns give the unit vector of the measured components for a point near Muzaffarabad.

Muzaffarabad-Balakot 25 km-long portion where greater displacements occur. The largest displacements are concentrated on this part of the hanging wall and probably explains why Balakot and Muzaffarabad were the cities most affected by the earthquake. North of Balakot, displacements decrease abruptly, but there is still a diffuse zone of displacement (dominated by uplift) suggesting slip on a deeper fault. This zone coincides with the IKSZ and is also the area where most of the aftershocks occur.

[9] It is noteworthy that from north to south, there are changes in the direction of horizontal motion in the hanging wall. Approximately north of a line joining the epicenter to Muzaffarabad, displacements involve nearly pure thrust motion toward the SW. To the south, there is a progressive rotation of displacements toward the south implying a significant increase of the right-lateral slip and consequently some along-strike extension in the hanging wall. However, close to the fault trace, the right-lateral component tends to decrease. This observation is consistent with the Harvard and NEIC moment tensor solutions that indicate a right lateral component of the slip. In contrast, displacement in the footwall are more uniformly toward the north-east.

[10] Existence of surface rupture suggested by the presence of high gradients of displacement in Figures 2 and 3 is supported by high resolution Quick-Bird optical imagery analysis. Comparing pre- and post-event 60 cm resolution images, evidence of surface rupture can be found at several locations on the inferred fault trace. Figures 3b and 3c–3d illustrate two examples of surface ruptures. One is north of Muzaffarabad near the Neelum river and corresponds to a

scarp, which is one of those recognized in the field and reported to be coseismic [see *Yeats et al.*, 2006, Figure 1].

#### 4. Slip Distribution Model

[11] To model static deformation on the fault, we used a homogeneous linear elastic halfspace model assuming that the fault dislocation is a rectangular plane reaching the surface [Okada, 1985]. Slip distribution is estimated in two steps. First, the geometry of the fault plane is optimized assuming uniform slip and looking for a global minimum misfit with the offset data (that are downsampled using a quad-tree algorithm to about 2000 points per data set). The minimum misfit is found for the following parameters: strike  $321.5^\circ$ , dip  $31.5^\circ$ , depth 0–10 km, length 74 km. Second, this fault plane is then extended along strike and down dip to give a length of 100 km and a width of 30 km (corresponding bottom depth is 15.7 km, see Figure 3 and auxiliary material Figure S3 for location) and subdivided into 2 by 2 km patches. We then invert for the slip distribution with the same data, solving for the dip-slip and strike-slip motion of each patch and applying a Laplacian smoothing constraint to prevent unrealistic oscillations. This approach using a non-negative least-squares algorithm is described in more detail by *Funning et al.* [2005]. Note that due to the curved geometry of the real fault trace, some data points are on the wrong side of our simplified fault plane model. Such points are masked out in this second step. Among the solutions found for different smoothing factors we select the one shown in Figure 4,

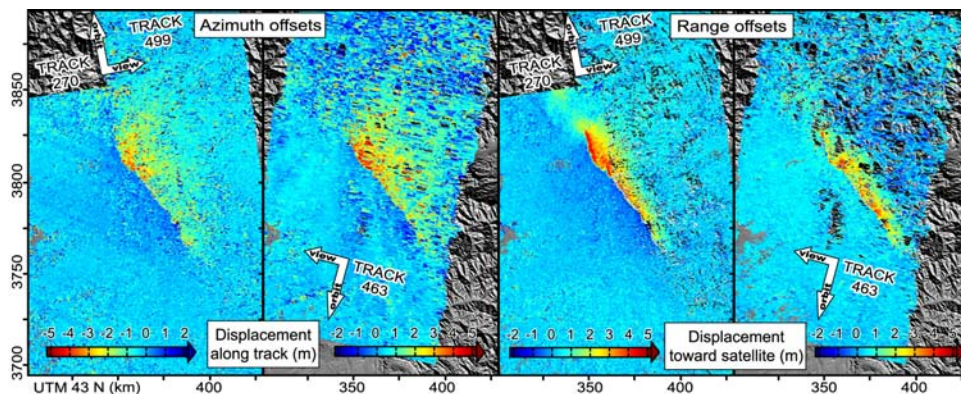


**Figure 2.** Azimuth and range offset measurements from ASAR ENVISAT images geocoded at 120 m resolution (range offsets are positive for a displacement toward the satellite). One descending and two ascending tracks are used to cover the epicentral area. Coseismic displacements of several meters, consistent with a NE-dipping thrust fault, are clearly visible at the center of the figure where the sharp color discontinuity delineates a highly deformed hanging wall to the east from a slightly deformed footwall to the west.

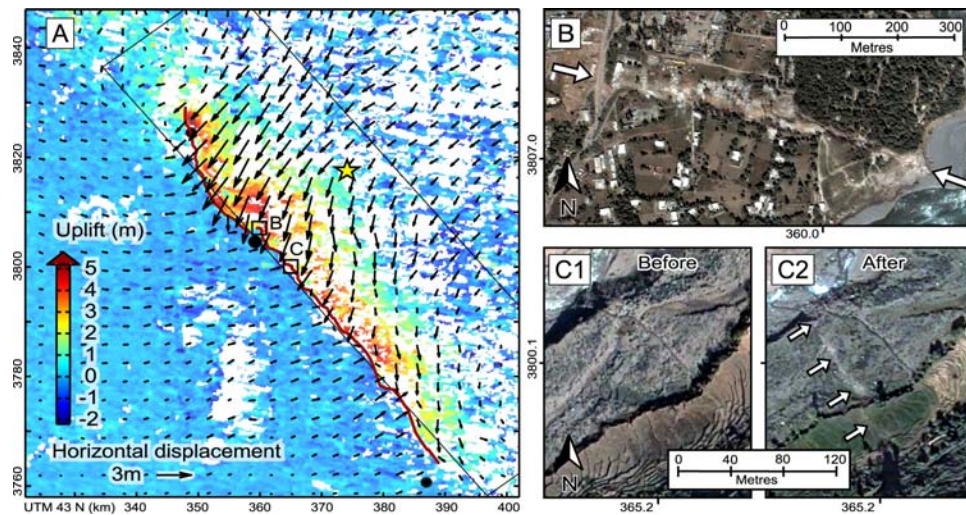


**Figure 3.** (A) 3D surface displacement field constructed from azimuth and range offset data sets. Arrows indicate horizontal displacements, and colors vertical displacements. Arrows are every 3.5 km and corresponds to the average displacements over a 4 km window (masking footwall data for hanging wall arrows and conversely for footwall arrows). From north to south, the black circles are the cities of Balakot, Muzaffarabad and Bagh. The squares indicate the location of the Quickbird imagery extracts (on the right side) showing evidences of surface rupture. The red line shows surface rupture trace inferred from satellite imagery (SAR, Quickbird and Landsat). The star is the NEIC epicenter and the thin black lines show the map projection of the plane used to model the fault. (B) Surface rupture located north of Muzaffarabad on the eastern bank of the Neelum river. Images (C1) before and (C2) after the earthquake showing the coseismic formation of a new fault scarp in the river bed of a tributary of the Jhelum river on the eastern flank of the valley.

based on a trade-off between high RMS misfit/low smoothness and low RMS misfit/high smoothness and on the minimization of the seismic moment (auxiliary material Figures S4a and S4b). The corresponding moment is  $3.36 \times 10^{20}$  N.m, which is larger than the moment of the Harvard CMT solution ( $2.94 \times 10^{20}$  N.m). The global RMS misfit to the whole data set is  $\sim 58$  cm and the 3D surface displacements constructed from the model show similar pattern to the one described in Figure 3 (see auxiliary material Figures S5, S6 and S7 for details). In order to estimate error on the model, the same inversion is applied to 100 data sets perturbed by introducing noise with characteristics similar to the noise found in the data. For each patch of the fault plane, the standard deviation of the 100 solutions gives an error estimation, which increase with depth up to 1.5 m (for details, see *Funning et al.* [2005] and auxiliary material Figure S8).

[12] The slip distribution pattern shows a main zone of slip larger than 6 m with a peak slip of 9.6 m ( $\pm 1.1$  m) at 4 km depth, located beneath the Muzaffarabad-Balakot segment. Beneath the southern segment, smaller slip occurs distributed on a second zone elongated along strike with a peak slip up to 7 m at 4 km depth. Slip larger than 3 m occurs down to depth of about 13 km ( $\pm 1$  km). The zone of maximum slip in our model is located further north than in the slip distribution derived by *Avouac et al.* [2006] from seismic waveforms and slip measurements at the fault trace (from correlation of optical satellite images). The difference is more pronounced when comparing with their slip distribution derived from the modeling of seismic waveforms alone. This suggests that geodetic measurements consistently indicate a zone of maximum slip within the Muzaffarabad-Balakot segment. In this part of the fault, our slip distribution shows more slip at depth than in their model, which

could be explained by the different spatial coverage of the geodetic data used in the two studies, the surface measurements of *Avouac et al.* [2006] being limited to the fault trace. Alternatively, the geometry of the modeled fault plane could also account for the difference: *Avouac et al.* [2006] use a two segments geometry that follows more closely the fault trace in its northern part than in our study that used a single plane and consequently could require more slip at depth.

## 5. Discussion and Conclusion

[13] Using SAR offsets we have extracted a synoptic view of the surface displacements covering the whole epicentral area of the Kashmir earthquake. From simple

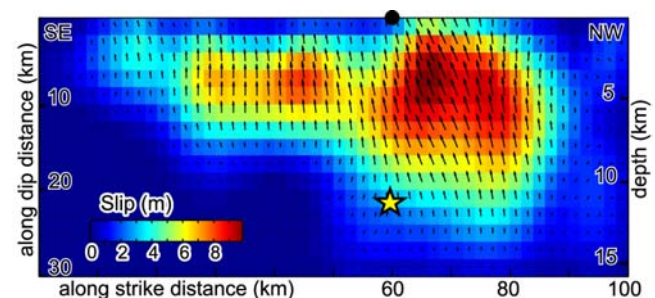


**Figure 4.** Slip distribution for a fault plane 100 km long, 30 km wide and dipping  $31.5^\circ$ NE (see location on Figure 3), inverted from the azimuth and range offset data sets. Magnitude of displacement is represented by color and slip vectors by the arrows. The star is the projection on the fault plane of the NEIC epicenter. The black dot represents the city of Muzaffarabad.

elastic modeling, we have estimated the slip distribution on the fault plane, which is able to reproduce the main features of the observed displacements. This spatially detailed analysis allows comparison with geological features that could have influenced the rupture process.

[14] The slip distribution shows that most of the slip corresponds to the rupture of the Balakot-Muzaffarabad northern segment. The left-step between the northern and southern fault segments is aligned with the North-South Jhelum valley southward of Muzaffarabad. *Tapponnier et al.* [2006], from geomorphic analysis, suggested that this left step could result from current left-lateral motion of the Jhelum fault, which runs along this valley. Another coincidence between slip distribution and geological features is that the fault trace follows more or less the MBT trace in its northern part and that displacements decrease abruptly north of Balakot where there is a dramatic bend of the MBT.

[15] All these observations are consistent with previous observations suggesting that the location of the rupture initiation or arrest tends to be at the location of intersecting faults or other features, implying a structural control on the slip distribution [e.g., *Manighetti et al.*, 2005]. In the case of the Kashmir earthquake, the hypocenter located at the down-dip edge of the zone of maximum slip is also at the transition zone between the two segments. However, such interpretation should be taken with caution as large errors can affect the hypocenter location (its depth  $\sim 12$  km is estimated from projection of the NEIC epicenter on the model fault plane).

[16] Regarding the zone of diffuse displacement observed north of Balakot that also coincide with the main concentration of aftershocks, triggered slip on a deeper part of the IKSZ ramp can be invoked. The data set used in this study does not allow us to discriminate between early post-seismic or coseismic deformation, as our first post-event image of that area was acquired on the 12th of November. This question deserves further investigations into the possible continuation of post-seismic displacements.

[17] Finally, we emphasize that for large ( $M > 6$ ) shallow continental earthquakes, the robust, all-weather SAR correlation technique can be applied to produce precise fault locations and preliminary displacement maps, just days after post-event image acquisition using ESA crisis procedure for data distribution. The potential of remote sensing analysis, such as that described here, for operational use in the relief effort or rapid scientific investigation (such as postseismic study) should not be overlooked.

[18] **Acknowledgments.** This research has been supported by the UK Natural Environment Research Council through COMET. TJW is supported

by a Royal Society University Research Fellowship. Part of this research was performed at the Jet Propulsion Laboratory, Caltech, under contract with NASA. We are grateful to the European Space Agency for providing the ENVISAT data used in this study (project AOE-621 and AOE-668). We thank Gareth Funning, who wrote parts of the code used for the slip inversion, and Nicola Capes of Nigel Press Associates for her help in obtaining the Quickbird imagery. We thank J. P. Avouac and two anonymous reviewers for helpful comments.

## References

- Armbruster, J., L. Seeber, and K. H. Jacob (1978), The northwestern termination of the Himalayan mountain front: Active tectonics from micro-earthquakes, *J. Geophys. Res.*, *83*(B1), 269–282.
- Avouac, J.-P., F. Ayoub, S. Leprince, O. Konca, and D. V. Helmberger (2006), The 2005, Mw 7.6 Kashmir earthquake: Sub-pixel correlation of ASTER images and seismic waveforms analysis, *Earth Planet. Sci. Lett.*, *249*(3–4), 514–528, doi:10.1016/j.epsl.2006.06.025.
- Bilham, R. (2004), Earthquakes in India and the Himalaya: Tectonics, geodesy and history, *Ann. Geophys.*, *47*, 839–858.
- Fujiwara, S., et al. (2006), Satellite data give snapshot of the 2005 Pakistan earthquake, *Eos Trans. AGU*, *87*(7), 73–84.
- Funning, G. J., B. E. Parsons, T. J. Wright, J. A. Jackson, and E. J. Fielding (2005), Surface displacements and source parameters of the 2003 Bam (Iran) earthquake from Envisat advanced synthetic aperture radar imagery, *J. Geophys. Res.*, *110*, B09406, doi:10.1029/2004JB003338.
- Manighetti, L., M. Campillo, C. Sammis, P. M. Mai, and G. C. P. King (2005), Evidence for self-similar, triangular slip distributions on earthquakes: Implications for earthquake and fault mechanics, *J. Geophys. Res.*, *110*, B05302, doi:10.1029/2004JB003174.
- Michel, R., J.-P. Avouac, and J. Taboury (1999), Measuring ground displacements from SAR amplitude images: Application to the Landers earthquake, *Geophys. Res. Lett.*, *26*(7), 875–878.
- Nakata, T., H. Tsutsumi, S. H. Khan, and R. D. Lawrence (1991), *Active Faults of Pakistan*, 141 pp., Res. Cent. for Reg. Geogr., Hiroshima Univ., Hiroshima, Japan.
- Okada, Y. (1985), Surface deformation due to shear and tensile faults in a half-space, *Bull. Seismol. Soc. Am.*, *75*(4), 1135–1154.
- Parsons, T., R. S. Yeats, Y. Yagi, and A. Hussain (2006), Static stress change from the 8 October, 2005  $M = 7.6$  Kashmir earthquake, *Geophys. Res. Lett.*, *33*, L06304, doi:10.1029/2005GL025429.
- Rosen, P. A., S. Hensley, I. R. Joughin, F. K. Li, S. N. Madsen, E. Rodriguez, and R. M. Goldstein (2000), Synthetic aperture radar interferometry, *Proc. IEEE*, *88*(3), 333–382, doi:10.1109/5.838084.
- Rosen, P. A., S. Hensley, G. Peltzer, and M. Simons (2004), Updated repeat orbit interferometry package released, *Eos Trans. AGU*, *85*(5), 47.
- Tapponnier, P., G. C. P. King, and L. Bollinger (2006), Active faulting and seismic hazard in the western Himalayan syntaxis, Pakistan, in *International Conference on 8 October 2005 Earthquake in Pakistan*, edited by A. B. Kausar, T. Karim, and T. Khan, pp. 2–3, Geol. Surv. of Pakistan, Quetta, Pakistan.
- Wright, T. J., B. E. Parsons, and Z. Lu (2004), Toward mapping surface deformation in three dimensions using InSAR, *Geophys. Res. Lett.*, *31*, L01607, doi:10.1029/2003GL018827.
- Yeats, R. S., A. B. Kausar, and T. Nakata (2006), Conferees examine deadly 2005 Kashmir earthquake, *Eos Trans. AGU*, *87*(11), 115.

B. E. Parsons, E. Pathier, R. Walker, and T. J. Wright, Centre for the Observation and Modelling of Earthquakes and Tectonics (COMET), Department of Earth Sciences, University of Oxford, Parks Road, Oxford OX1 3PR, UK. (erwan.pathier@earth.ox.ac.uk)

E. J. Fielding and S. Hensley, Jet Propulsion Laboratory, M.S. 300-233, California Institute of Technology, 4800 Oak Grove Drive, Pasadena, CA 91109, USA.